https://doi.org/10.5194/nhess-2019-342
Preprint. Discussion started: 27 November 2019

Natural Hazards and Earth System Sciences
Discussions

Brief Communication: An Electrifying Atmospheric River: Understanding the Thunderstorm Event in Santa Barbara County during March 2019

Deanna Nash[1] and Leila M.V. Carvalho[1,2]

[1]Department of Geography, University of California, Santa Barbara, CA 93106 USA
[2]Earth Research Institute, University of California, Santa Barbara, CA 93106, USA

Correspondence: Deanna Nash (dlnash@ucsb.edu)

Abstract. On 5 March 2019 12 UTC, an Atmospheric River (AR) made landfall in Santa Barbara, CA and lasted approximately 30 hours. This AR was one of many that occurred during the winter season in Santa Barbara. However, during this AR, a massive number of lightning pulses were detected by Earth Networks Global Lightning Network (ENGLN) near and off the coast of Santa Barbara, CA. In the 24 hours following 6 March 2019 00 UTC, 14,416 lightning flashes occurred around southern California (140°W to 110°W and 20°N to 50°N). This far exceeded the climatological average number of lightning flashes recorded by the Lightning Imaging Sensor (LIS) and Optical Transient Detector (OTD) on the Tropical Rainfall Measuring Mission (TRMM). Between the years of 1995 and 2014, the TRMM LIS-OTD detected an average flash density of approximately 9.15 flashes per day in the same region around southern California. While the AR could be considered part of a typical winter storm in the area, the extraordinary amount of lightning strikes in the region was very anomalous. This combined thunderstorm and Atmospheric River event resulted in 36-hour precipitation totals in Santa Barbara to be approximately 77.6 mm, with a maximum rain rate of 16.5 mm hr^{-1}. This article describes the synoptic and mesoscale characteristics of this electrifying AR event.

1 Introduction

Due to recent wildfire activity in Santa Barbara county (e.g. Thomas Fire during December 2017, Whittier Fire during July 2017, and Sherpa Fire during June and July 2016) this region is at high risk for post-fire debris flow when 15 minutes of rainfall has an intensity greater than or equal to 24 mm $hour^{-1}$ (USGS, 2019). These conditions were observed during the devastating Montecito debris flow on the 9 January 2018 that resulted in 23 deaths, 246 structures destroyed, and 167 damaged structures (Oakley et al., 2018). On 1 March 2019, the National Weather Service (NWS) in Oxnard, CA forecasted 2 storms to hit Santa Barbara County (1-2 March 2019 and 5-6 March 2019). Approximately 17.5 mm of rain fell in Santa Barbara during the storm on 2 March 2019 based on Global Precipitation Measurement (GPM) precipitation (Huffman et al., 2019). On 5 March 21 UTC, a mandatory evacuation order was employed for the Thomas, Whittier, and Sherpa fire burn areas due to the prediction of a subsequent severe storm and the flood potential that existed for low-lying areas given increased ground saturation from the storm on 2 March 2019, impacting about 3,000 residents. While no significant debris flows were triggered during this event,

https://doi.org/10.5194/nhess-2019-342
Preprint. Discussion started: 27 November 2019


Natural Hazards and Earth System Sciences
Discussions

a combination of an Atmospheric River (AR) event and an extreme number of lightning strikes made this storm exceptional. Figure 1a shows a photo of lightning strikes at the Santa Barbara Harbor during the storm taken by Santa Barbara County Fire Department's Mike Eliason.

On 5 March 2019 12 UTC, an AR made landfall on the Santa Barbara coast (34.5°N, 119.5°W) and lasted 30 hours. During the AR event, between 5 March 12 UTC and 6 March 18 UTC, the total accumulated precipitation was approximately 77.6 mm in Santa Barbara (Fig. 1b), with the highest rain rate of 16.5 mm hour^{-1} at 6 March 2019 04:30 UTC based on GPM (Huffman et al., 2019). While this was not enough precipitation to initiate debris flow, instances of hail were identified by the National Oceanic and Atmospheric Administration (NOAA) Next Generation Radar Level 3 (NEXRAD L3) hail signature product (see Fig. 1b). The presence of hail indicates strong updrafts and a low freezing level, which are conditions that also favor the development of lightning in a storm (Pruppacher and Klett, 1997). During this AR event, Earth Networks Global Lightning Network (ENGLN) detected 73,442 flashes of lightning with 119,363 combined in-cloud (IC) and cloud-to-ground (CG) pulses around Southern California (140°W to 110°W and 20°N to 50°N) (Earth Networks, 2019). Among these, 50,399 pulses occurred in the 24 hour period following 6 March 2019 00 UTC (Fig. 1c). There were 533 CG pulses and 953 IC pulses over Santa Barbara county on 6 March 2019. The strongest positive flash over Santa Barbara county was CG with a peak current of 127,212 amps located east of Cachuma Lake at 34.59°N and 119.79°W at 6 March 2019 05:48 UTC. At 6 March 2019 04:06 UTC, the strongest negative CG flash over Santa Barbara county occurred in Los Padres National Forest at 34.61°N and 119.52°W at a peak current of -223,036 amps.

According to the Tropical Rainfall Measuring Mission Lightning Imaging Sensor and Optical Transient Detector (TRMM LIS-OTD) Lightning Climatology, there were, between 1995 and 2014, an average of 9.15 flashes per day in the region surrounding southern California (140°W to 110°W and 20°N to 50°N) (Fig. 1d) (Cecil, 2015). Based on the AR database of Guan and Waliser (2015), there were on average 10 AR days occurring between December and March each year in Santa Barbara, with a total of 742 ARs that made landfall in the grid cells closest to Santa Barbara. When compared to the TRMM LIS-OTD low resolution time series, between 1995 and 2014 there were approximately 350 landfalling AR events that coincided with lightning flashes, with the majority of events resulting in less than 60 flashes per day (Cecil, 2015). While there was minimal damage regarding the storm (e.g. small lightning fires, power outages), this event was meteorologically significant, specifically because of the number of lightning strikes in such a short period. This paper describes the synoptic and mesoscale dynamics that caused the extreme number of lightning strikes to occur in a region that historically has seen little to no lightning. In addition, this paper explains the interaction of the AR that simultaneously occurred with the hail and lightning, resulting in precipitation.

2 Data and Methods

Climate Forecast System version 2 (CFSv2) (Saha et al., 2014) operational analysis was used in this study to evaluate the synoptic and mesoscale meteorological conditions between 10°N and 50°N and 150°W to 110°W between the dates 4 March 2019 18 UTC and 6 March 2019 18 UTC. CFSv2 data at 0.5°x 0.5°horizontal resolution was obtained at 37 pressure levels

https://doi.org/10.5194/nhess-2019-342
Preprint. Discussion started: 27 November 2019

Natural Hazards and Earth System Sciences
Discussions
Open Access
EGU

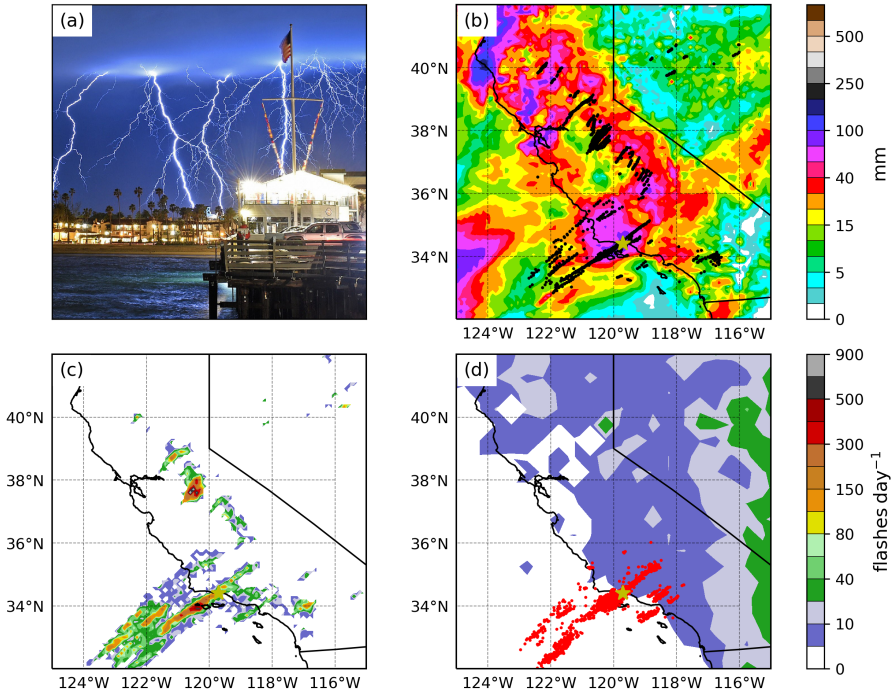

Figure 1. (a) Photo of lightning at the Santa Barbara Harbor in Santa Barbara, CA taken by Mike Eliason from the Santa Barbara County Fire Department during the storm at 6 March 2019 04 UTC. (b) GPM precipitation totals (shaded; mm) and locations of NOAA NEXRAD L3 Hail Signatures (black points) between 5 March 2019 12 UTC and 6 March 2019 23:59 UTC. The location of Santa Barbara is indicated by the gold star. (c) ENGLN lightning strike frequency (shaded; flashes day^{-1}) on 6 March 2019. The location of Santa Barbara is indicated by the gold star. (d) Climatological mean lightning density (shaded; flashes day^{-1}) between 1995 and 2014 using TRMM LIS-OTD lightning climatology and lightning strike locations (red points) between 04 and 05 UTC on 6 March 2019 based on ENGLN. The location of Santa Barbara is indicated by the gold star.

between 1000 hPa and 1 hPa at a 6-hourly time scale. AR conditions are determined based on IVT (see appendix for calculation) exceeding 250 kg m^{-1} s^{-1} at a fixed geographical point. The AR event in this study refers to the time that the AR conditions occurred in Santa Barbara, i.e. at the grid cell centered on 34.5°N and 119.5°W. The duration of the AR event is determined by the time (in hours) that the AR conditions are consecutively met. The other calculated variables from CFSv2 are dew point (Td) and equivalent potential temperature (ϑ_e), which are calculated based on Bolton (1980, eq. 11, 43).

Lightning flash data obtained from Earth Networks Global Lightning Network (Earth Networks, 2019) was used to quantify the location and number of lightning strikes between 4 March 2019 00 UTC and 7 March 2019 00 UTC near southern California. The global lightning network, which includes more than 1,700 sensors, detects lightning flashes and various information about those flashes, including the latitude, longitude, amplitude of the lighting, duration of the flash, and the number of IC and CG pulses within a given flash (Earth Networks, 2019). A lightning flash can be made up of one or more IC or CG lightning pulses, which connect regions of opposite polarity (+/-). To put the extremity of this lightning event into climatological con-

https://doi.org/10.5194/nhess-2019-342
Preprint. Discussion started: 27 November 2019


Natural Hazards and Earth System Sciences
Discussions

text, an annual lightning strike climatology from Tropical Rainfall Measuring Mission Lightning Imaging Sensor and Optical Transient Detector (TRMM LIS-OTD) (Cecil, 2015) was used at a horizontal resolution of 0.5°by 0.5°between 1995 and 2014 for the region surrounding southern California. TRMM LIS-OTD records an area climatological average of 9.15 flashes per day in the region surrounding southern California, making the 14,416 lightning flashes in under 24 hours very extreme. In fact, if this was the only lightning activity for 2019, it would represent about 1,500 times the climatological rate.

For precipitation, data from NASA's Global Precipitation Measurement mission (GPM) was used at a 30-minute temporal resolution between the dates 2 March 2019 00 UTC and 6 March 2019 23:59 UTC at a 0.1°gridded resolution (Huffman et al., 2019). To identify the approximate location, time, and diameter of hail, National Oceanic and Atmospheric Administration's Next Generation Radar Level 3 (NOAA's NEXRAD L3) hail signature product was used (NOAA National Weather Service (NWS) Radar Operations Center, 2019). To identify cloud convection and cloud top height via cloud top temperature, the Cloud and Moisture Imagery (CMI) product from GOES-R (GOES-17) Advanced Baseline Imager Level 2 was obtained for 6 March between 03 UTC and 05 UTC at 5-minute temporal intervals and 10 km by 10 km spatial resolution (GOES-R Algorithm Working Group and GOES-R Series Program, 2017).

3 Results and Discussion

3.1 Extratropical Cyclone and AR Conditions

To understand why the lightning happened at such an extreme rate in a region that sees little to no lightning, the synoptic conditions for this event are described. Lightning usually occurs when the electric charges in a cloud separate and exceed the intensity that the air can sustain (Price, 2013). Charges usually build up in the mixed phase region of the clouds (0°C to -40°C) when there are sufficient updrafts to lift particles above the freezing level (Price and Rind, 1993). The synoptic conditions of this event show that the cyclogenesis combined with the dynamical lift of the AR via the warm conveyor belt (WCB) provided enough updraft to aid in the electrification of the clouds.

Following an extratropical cyclone that made landfall at 1 March 2019 12 UTC, a deep mid-level (500 hPa) trough developed into a closed low system, forming a pool of cold air centered at approximately 32°N and 140°W by 4 March 18 UTC (Fig. 2a). The surface low-pressure was located directly below the 500 hPa closed low on 4 March 18 UTC (Fig. 2a). This mid-level closed low moved eastward and northward, until 6 March 12 UTC when it was no longer closed (Fig. 2h). According to Oakley and Redmond (2014), 41-50% of precipitation in Santa Barbara between October and March is associated with closed lows. The surface low-pressure deepened from 1005 hPa to approximately 996.36 hPa by the peak event time at 6 March 2019 06 UTC, at which point it was centered around 38°N and 126°W, west of northern California (Fig. 2g). At the peak time of the event, 6 March 06 UTC, the jet streak exit region was located at 35°N and 122°W, directly northwest of Santa Barbara (Fig. S1g). Vertical velocity peaked in Santa Barbara on 6 March 06 UTC with a value of 0.35 m s^{-1} indicating strong upward motion (Fig. S2g). Off the coast at 34°N and 121.5°W, vertical velocity reached 0.9 m s^{-1} at 6 March 06 UTC (Fig. S2g).

These synoptic conditions provided the dynamical mechanisms necessary for subtropical moisture to be transported via an AR, shown as the area of IVT greater than 250 kg m^{-1} s^{-1} (Fig. 2). This AR made landfall at approximately 5 March 12 UTC on

https://doi.org/10.5194/nhess-2019-342
Preprint. Discussion started: 27 November 2019

Natural Hazards and Earth System Sciences
Discussions

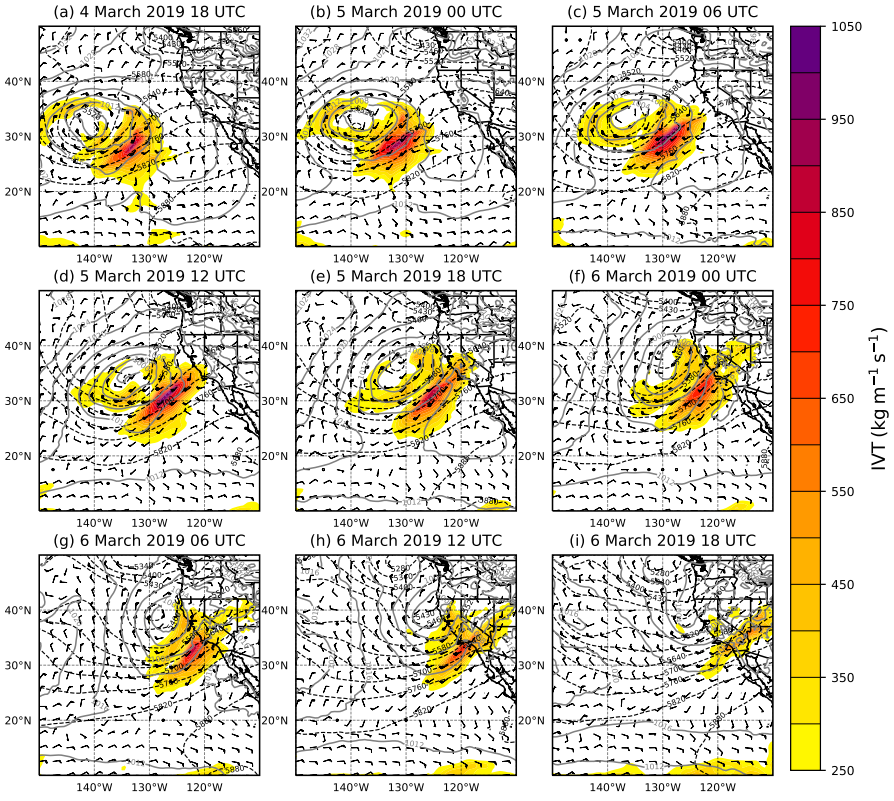

Figure 2. CFSv2 data showing IVT (shaded; kg m^{-1} s^{-1}), 850 hPa wind (barbs; knots), Mean sea level pressure (grey contours; hPa), and 500 hPa geopotential height (black dashed contours; m) at 6-hourly time steps between 4 March 2019 18 UTC and 6 March 2019 18 UTC. The time step closest to the peak of the event is shown in figure (g) at 6 March 2019 06 UTC in the bottom left corner.

the west coast near Santa Barbara and lasted approximately 30 hours (Fig. 2d-i). For the duration of the event, the AR had an average IVT value of 395 kg m^{-1} s^{-1} with a maximum value of 735 kg m^{-1} s^{-1}) in the grid cell closest to Santa Barbara (34.5°N and 119.5°W) (Fig. S3). Based on the duration (30 hours) and maximum instantaneous IVT intensity of the AR (735 kg m^{-1} s^{-1}), this event is categorized at AR-CAT 2 according to Ralph et al. (2019), indicating that this AR was most likely beneficial with a possibility of being hazardous. Most thunderstorms are associated with high values of Convective Available Potential Energy (CAPE), which measures the amount of energy available for convection. While this storm had values of surface-based CAPE up to 1000 J kg^{-1} as it made its way across the Pacific Ocean toward the west coast of California, at the time closest to the peak of the event, there was little to no CAPE in Santa Barbara (10 J kg^{-1}) where lightning occurred (Fig. S4). However, like the extreme precipitation events in Cannon et al. (2018), additional dynamical forcing can develop convection even when CAPE is low.

Equivalent potential temperature at 850 hPa (ϑ_e) (Fig. S5) identifies the formation of the warm conveyor belt (WCB), or the ascending air within the warm sector of the extratropical cyclone between 5 March 12 UTC and 6 March 12 UTC (Browning,

https://doi.org/10.5194/nhess-2019-342
Preprint. Discussion started: 27 November 2019


Natural Hazards and Earth System Sciences
Discussions

1986; Dettinger et al., 2015). At 6 March 06 UTC (Fig. S5g), the cold front lies along the densely packed isotherms between the coast of California and 32°N and 124°W, and the warm front is located parallel to the coast of California. This placed the region of warm air advection and the WCB in the southern region of the domain between the two fronts where ϑ_e is around 320 K. Water vapor in the AR, which can be sourced from intense vapor transport out of the tropics as well midlatitude convergence of water vapor along the path of the AR, was transported via winds into the WCB (Dettinger et al., 2015). The uplift of the moisture from the AR most likely occurred due to orographic uplift from interaction with complex topography as well as dynamic uplift from the WCB (Fig. S2, S5). It has been suggested that WCBs and ARs can form on their own without direct connection to each other (Dettinger et al., 2015; Dacre et al., 2019). In our case, the combination of the AR with the WCB resulted in updrafts as well precipitation and hail formation.

3.2 Precipitation and Hail

Wind in the skew(t) - log(p) diagram at 34.5°N 119.5°W (Fig. 3a) for the time closest to the peak of the event (6 March 06 UTC) indicates strong warm air advection below 800 hPa. This strong veering profile near the surface with increasing wind speeds with height intensifies the mesocyclone and maintains the storm. At the surface, although Convective Available Potential Energy (CAPE) was low (10 J kg^{-1}), the proximity of temperature and dew point profiles place the Lifting Condensation Level (LCL) very close to the surface (Fig. 3a). These factors combined with the vertical velocity of 0.35 m s^{-1} (Fig. S2g) in Santa Barbara resulted in precipitation. At the time closest to the peak of the event (6 March 06 UTC), a band of precipitation parallel to the cold front is associated with the AR (Fig. S2g). In the Santa Barbara region, GPM measured peak rain rate values at about 16.5 mm $hour^{-1}$, with the 36-hour rain totals of about 77.6 mm (Fig. 1b). GOES-17 Cloud and Moisture Imagery Brightness Temperature (Fig. S6) indicates vigorous convection via cold cloud temperatures that decrease to approximately -71°C near Santa Barbara. These temperatures indicate a very strong updraft where they occur, which would result in hail formation when water droplets in the region of the updraft are carried above the freezing level (Wallace and Hobbs, 2006; Pruppacher and Klett, 1997).

Between 800 hPa and 625 hPa, parcels are extremely moist (the dew point is equal to the temperature), indicating the high moisture from the AR (Fig. 3a, b). Precipitation resulted from the moisture from the AR being lifted via the WCB (Fig. S2, S5). Figure 3b shows the vertical profile of horizontal water vapor flux (m s^{-1}) on 6 March 06 UTC at 34.5°N, 119.5°W, showing that the water vapor flux peaked at 0.17 m s^{-1} between 700 and 800 hPa. Compared to the climatological vertical profile of water vapor flux from the past 170 AR events in Santa Barbara, the AR on 6 March 2019 was extremely moist and peaked at an altitude closer to the surface. The height (km above mean sea level) of the 0°isotherm at 34.5°N, 119.5°W (Fig. 3c) is located between 2.5 km and 4 km above mean sea level for the duration of the storm, which is roughly below 700 hPa. Therefore, the moisture that was being transported in via the AR was lifted by strong updrafts in a below freezing level environment (Fig. 3b, 3c) which contributed to the formation of hail with an average size of 13.5 mm (Fig. 1b) due to the low freezing level (Fig. 3c). When compared to the hail locations from NOAA's NEXRAD L3 hail signatures, the location of the hail is co-located with the cold cloud top temperature.

https://doi.org/10.5194/nhess-2019-342
Preprint. Discussion started: 27 November 2019

Natural Hazards and Earth System Sciences
Discussions
Open Access
EGU

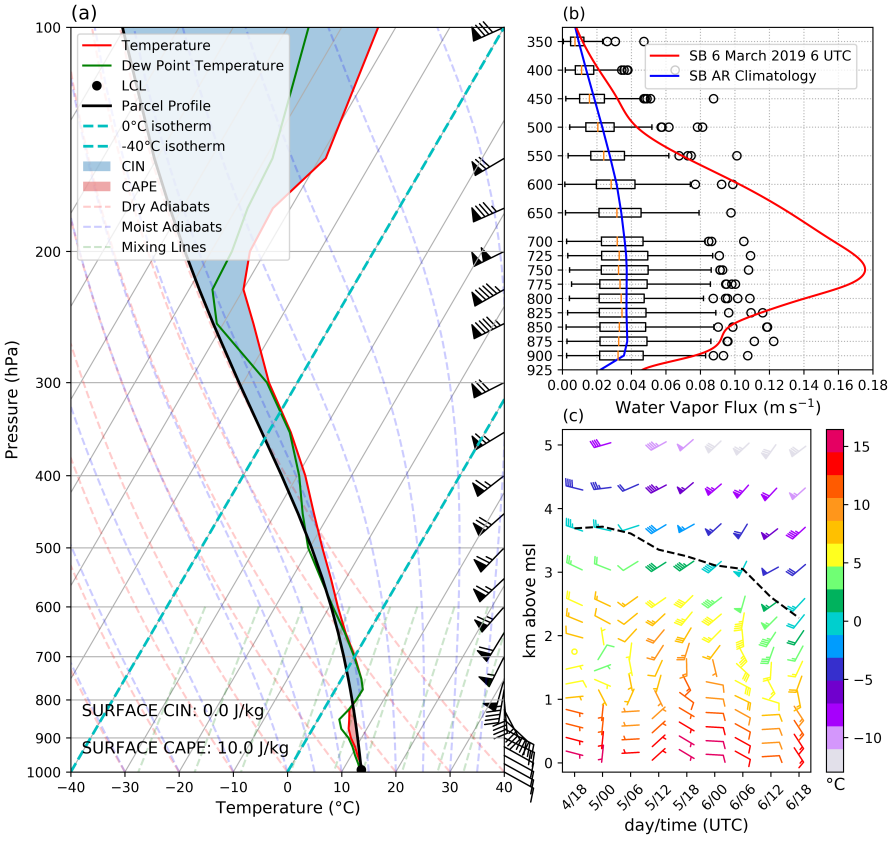

Figure 3. (a) Skew(t) - log(p) vertical profile of CFSv2 temperature (red line) and dew point (green line) at 34.5N and 119.5W at 6 March 2019 06 UTC. CFSv2 winds (knots; barbs) are indicated on the right side of the figure for each vertical level. The thermodynamic profile of the parcel is indicated by the solid black line. CAPE is indicated as the red shaded region and Convective Inhibition (CIN) is indicated by the blue shaded region. (b) Climatological vertical profile of horizontal water vapor flux (m s^{-1}) based on MERRA2 at 34.5°N, 119.375°W for all days when AR conditions are met during the month of March between 1980 and 2015 (i.e. IVT >= 250 kg m^{-1} s^{-1}) at this location (blue line and box and whisker plots show the distribution of the 170 events), and vertical profile of horizontal water vapor flux (m s^{-1} based on CFSv2 at the same location at 6 March 2019 06 UTC. (c) CFSv2 winds (knots, barbs) at vertical levels (km above mean sea level) at 34.5°N and 119.5°W at 6-hour intervals from 4 March 2019 18 UTC to 6 March 2019 18 UTC. The temperature (°C) is indicated by the color of the barb. The height of the 0°C isotherm is indicated by the black dashed line.

3.3 Lightning Conditions

The convective updraft in the lower troposphere was very important for the onset of electrification, or the build-up of regions with positive and negative net charges in the mixed-phase region of the cloud (0°C to -40°C), which results in lightning and thunder (Price and Rind, 1993; Price, 2013). Updrafts via convection transported smaller droplets to above the freezing level, located below 700 hPa, giving them a positive charge and formed hail (Fig. 3c, 1b) (Doswell, 2001; Price and Rind, 1993).

https://doi.org/10.5194/nhess-2019-342
Preprint. Discussion started: 27 November 2019

Natural Hazards and Earth System Sciences
Discussions

Figure 3a shows the skew(t) - log(p) plot at Santa Barbara at the time closest to the peak of the event (6 March 06 UTC) and indicates entrainment of dry air between 300 hPa and 200 hPa with fast winds of approximately 100 knots. This upper-level intrusion of dry, cold air via the larger scale extratropical cyclone's cold front possibly resulted in cold, descending air into the mixed phase region of the thunderstorm that negatively charged particles (Fig. 3a) (Price and Rind, 1993; Price, 2013). While clouds that have high lightning activity are usually associated with maximum updrafts (> 10 m s^{-1}), very little updraft was required to carry the particles to the mixed-phase region of this thunderstorm cloud because the freezing level was low (about 2.5 km above mean sea level) (Price, 2013).

When the updrafted droplets from the AR and WCB and the downdrafted hailstones collided and released latent heat, they would have potentially formed graupel, a softer form of hail that is warmer than their environment (Price and Rind, 1993; Doswell, 2001). The particles become positively charged when ascending or negatively charged when descending when they collide with graupel. Over time, this changed the storm cloud microphysics and charges resulting in a negatively charged base and a positively charged top (Doswell, 2001; Price, 2013). In-cloud (IC) lightning pulses transport charges between the positively charged region of the thunderstorm and the negatively charged region of the thunderstorm while cloud-to-ground (CG) lightning pulses transport negative charges from the lower to middle region of the thunderstorm to the ground (Price, 2013).

According to Price and Rind (1993), the proportion of IC to CG lightning pulses in thunderstorms is well correlated with the thickness of the cloud region between 0°C and the top of the cloud. Therefore, as the thickness of the thunderstorm cloud increases, the ratio of IC to CG also increases. Here we use cloud-top height from GOES-R (GOES-17) Advanced Baseline Imager Level 2 (Fig. S8) and the height of the 0°isotherm (Fig. S9) as a proxy for cloud thickness. Figure S7a shows the number of IC pulses and CG pulses at every 15 minutes between 4 March 00 UTC and 7 March 00 UTC in the region of the extratropical cyclone. Between 4 March 00 UTC and 12 UTC, there are between 2000 and 3000 CG pulses and about 1000 to 2000 IC pulses centered around 26°N and 136°W. The second peak in lightning occurs at approximately 5 March 12 UTC with almost 4000 CG pulses and 3000 IC pulses centered around 30°N and 128°W (Fig. S7a). The last peak of lightning occurred between 6 March 00 UTC and 06 UTC with approximately 3000 IC pulses and less than 1000 CG pulses centered at 34°N and 120°W (Fig. S7a). The cloud top height near the lightning throughout the event is between 9,000 m and 10,000 m (Fig. S8). However, the 0°isotherm near the lightning grows closer to the ground as time passes, indicating that the cloud thickness increases as the event progresses (Fig. S9). The height of the IC pulses are below 5000 m before 5 March 12 UTC and between 7500 and 10000 m after 5 March 18 UTC (Fig. S7b). The increased IC pulse height (Fig. S7b) can be accounted for because of the increased cloud thickness in the later half of the storm (after 5 March 18 UTC), similar to the findings of Price and Rind (1993). This shows that the increased moisture from the AR being lifted via the WCB and orographic uplift and the decreased freezing level from the large-scale cold front were critical in generating the conditions necessary for the exceptional amount of lightning that occurred.

https://doi.org/10.5194/nhess-2019-342
Preprint. Discussion started: 27 November 2019

Natural Hazards and Earth System Sciences
Discussions

4 Conclusions

On the coast of the Santa Barbara, CA region, an extratropical cyclone and an AR made landfall at 5 March 2019 12 UTC. The AR intensified until its peak at 6 March 2019 06 UTC, resulting in precipitation via uplift from the WCB. There were cold clouds and vigorous convection that reached its peak at 6 March 2019 04 UTC. According to GPM, precipitation in the Santa Barbara region reached its peak at approximately 04:30 UTC on 6 March 2019 at a rate of 16.5 mm hr^{-1}. The event total accumulated precipitation in the Santa Barbara region was 77.6 mm. In 30 hours between 5 March 12 UTC and 6 March 18 UTC, ENGLN detected 73,442 flashes of lightning with 119,363 combined in-cloud (IC) and cloud-to-ground (CG) pulses around Southern California. Of those, 1,486 lightning pulses occurred over Santa Barbara County in the 24 hours following 6 March 2019 00 UTC, 533 of which were cloud-to-ground.

It is highly unusual that lightning would occur in this region, let alone the sheer number of lightning strikes that have occurred. A co-occurring AR likely made the lightning event doubly unusual because of the heat and moisture the AR provides. This storm was a typical winter storm for the region of Santa Barbara, made unusual by the high water vapor content provided by the AR. This system developed in a cool environment due to the 0°C isotherm being close to the surface (approximately 2.5 km above mean sea level) with a great available moisture content from maximum IVT and event duration typical of AR category 2 (mean IVT = 395 kg m^{-1} s^{-1}, maximum IVT = 735 kg m^{-1} s^{-1}, duration = 30 hours). The unique combination of the cold environment with high moisture availability provided the ingredients to form hail. Dry air entrainment from the cold front at about 250 hPa enhanced downdrafts and the WCB that lifted the AR generated updrafts at 850 hPa. The combination of updrafts and downdrafts formed hail and helped to change the charge of the clouds to produce lightning. Understanding the dynamics of this storm provides the theoretical basis for future, systematic investigation of the relationship between ARs and unusual lightning scenarios in other regions. It also is critical to understand these processes in populated areas such as Santa Barbara, where lightning can significantly increase hazards during extreme rainfall events.

Code and data availability. The code for this analysis can be found at https://github.com/dlnash/arthunderstorm2019. May et al. (2008 - 2017) was used for the development of some of the figures. CFSv2 data (Saha et al., 2014, https://www.ncdc.noaa.gov/data-access/model-data/model-datasets/climate-forecast-system-version2-cfsv2), GPM data (Huffman et al., 2019, https://disc.gsfc.nasa.gov/datasets/GPM_3IMERGHH_06/summary), TRMM LIS-OTD lightning climatology (Cecil, 2015, https://ghrc.nsstc.nasa.gov/uso/ds_details/collections/loCv2.3.2015.html), GOES-R data (GOES-R Algorithm Working Group and GOES-R Series Program, 2017, https://data.nodc.noaa.gov/cgi-bin/iso?id=gov.noaa.ncdc:C01502), MERRA-2 data (Global Modeling and Assimilation Office (GMAO), 2015; Gelaro et al., 2017, https://disc.gsfc.nasa.gov/datasets/M2I6NPANA_V5.12.4/summary?keywords=MERRA2), and NOAA NEXRAD L3 data (NOAA National Weather Service (NWS) Radar Operations Center, 2019, https://data.nodc.noaa.gov/cgi-bin/iso?id=gov.noaa.ncdc:C00708) are all freely available online. The global AR database based on MERRA-2 and the detection algorithm from Guan and Waliser (2015) used to identify AR events between 1980 and 2019 are freely available at https://ucla.box.com/ARcatalog. The lightning data used for this study was freely provided by Earth Networks (Earth Networks, 2019).

https://doi.org/10.5194/nhess-2019-342
Preprint. Discussion started: 27 November 2019

Natural Hazards and Earth System Sciences
Discussions

Appendix A: Calculation of IVT

Integrated water vapor transport (IVT), a variable widely used for the detection and identification of ARs (e.g. (Guan and Waliser, 2015; Ralph et al., 2019; Dettinger et al., 2015)) is derived from specific humidity and wind fields at 17 pressure levels between 1,000 and 300 hPa inclusive from the CFSv2 operational analysis. IVT is calculated in the zonal (x) and meridional (y) direction using the following equations:

$$IVT_x = -\frac{1}{g}\int uqdp \tag{A1}$$

$$IVT_y = -\frac{1}{g}\int vqdp \tag{A2}$$

where g is the gravitational acceleration, u is zonal wind, v is meridional wind, q is specific humidity, p is pressure, and the column integration is between pressure levels 1000 and 300 hPa inclusive.

Author contributions. LC conceptualized this article and participated in the interpretation of the data. DN participated in data collection, analysis, interpretation, and drafting of the article. All authors participated in the revision and final version of the article.

Competing interests. The authors declare that they have no conflict of interest.

Acknowledgements. This research was supported by NASA Headquarters under the NASA Earth and Space Science Fellowship Program - Grant 80NSSC18K1412. The authors would like to thank Duane Waliser and Bin Guan at NASA's Jet Propulsion Laboratory in Pasadena, CA and Tessa Montini at University of California, Santa Barbara for insights into this event.

https://doi.org/10.5194/nhess-2019-342
Preprint. Discussion started: 27 November 2019

References

Bolton, D.: The Computation of Equivalent Potential Temperature, Monthly Weather Review, 108, 1046–1053, https://doi.org/10.1175/1520-0493(1980)108<1046:tcoept>2.0.co;2, 1980.

Browning, K. A.: Conceptual models of precipitation systems, Weather and Forecasting, 1, 23–41, https://doi.org/10.1175/1520-0434(1986)001<0023:CMOPS>2.0.CO;2, 1986.

Cannon, F., Hecht, C. W., Cordeira, J. M., and Ralph, F. M.: Synoptic and Mesoscale Forcing of Southern California Extreme Precipitation, Journal of Geophysical Research: Atmospheres, 123, 13–714, https://doi.org/10.1029/2018JD029045, 2018.

Cecil, D. J.: LIS/OTD Gridded Lightning Climatology Data Collection Version 2.3.2015, NASA EOSDIS Global Hydrology Resource Center Distributed Active Archive Center Huntsville, Alabama, U.S.A, accessed 20 August 2019, https://doi.org/http:/dx.doi.org/10.5067/LIS/LIS-OTD/DATA311, 2015.

Dacre, H. F., Martinez-Alvarado, O., and Mbengue, C. O.: Linking atmospheric rivers and warm conveyor belt airflows, Journal of Hydrometeorology, 20, 1183–1196, https://doi.org/https://doi.org/10.1175/JHM-D-18-0175.1, 2019.

Dettinger, M., Ralph, F. M., and Lavers, D. A.: Setting the stage for a global science of atmospheric rivers, Eos, Earth and Space Science News, 96, https://doi.org/10.1029/2015EO038675, 2015.

Doswell, C. A.: Severe convective storms—An overview, in: Severe convective storms, pp. 1–26, Springer, https://doi.org/https://doi.org/10.1007/978-1-935704-06-5_1, 2001.

Earth Networks: Earth Networks Global Lightning Network, https://www.earthnetworks.com/product/weather-sensors/lightning/, accessed: 18 July 2019, 2019.

Gelaro, R., McCarty, W., Suárez, M. J., Todling, R., Molod, A., Takacs, L., Randles, C. A., Darmenov, A., Bosilovich, M. G., Reichle, R., et al.: The modern-era retrospective analysis for research and applications, version 2 (MERRA-2), Journal of Climate, 30, 5419–5454, https://doi.org/10.1175/JCLI-D-16-0758.1, 2017.

Global Modeling and Assimilation Office (GMAO): MERRA-2 inst6_3d_ana_Np: 3d, 6-Hourly, Instantaneous, Pressure-Level, Analysis, Analyzed Meteorological Fields V5.12.4, Greenbelt, MD, USA, Goddard Earth Sciences Data and Information Services Center (GES DISC), accessed: 14 August 2019, 10.5067/A7S6XP56VZWS, 2015.

GOES-R Algorithm Working Group and GOES-R Series Program: NOAA GOES-R Series Advanced Baseline Imager (ABI) Level 2 Cloud and Moisture Imagery Products (CMIP) Band 13, NOAA National Centers for Environmental Information, https://doi.org/10.7289/V5736P36, access date: 22 July 2019, 2017.

Guan, B. and Waliser, D.: Detection of atmospheric rivers: Evaluation and application of an algorithm for global studies, Journal of Geophysical Research: Atmospheres, 120, 12 514–12 535, https://doi.org/10.1002/2015JD024257, 2015.

Huffman, G., Stocker, E., Bolvin, D., Nelkin, E., and Tan, J.: GPM IMERG Final Precipitation L3 Half Hourly 0.1 degree x 0.1 degree V06, Greenbelt, MD, Goddard Earth Sciences Data and Information Services Center (GES DISC), https://doi.org/10.5067/GPM/IMERG/3B-HH/05, accessed: 6 September 2019, 2019.

May, R., Arms, S., Marsh, P., Bruning, E., and Leeman, J.: MetPy: A Python Package for Meteorological Data, https://doi.org/10.5065/D6WW7G29, https://github.com/Unidata/MetPy, 2008 - 2017.

NOAA National Weather Service (NWS) Radar Operations Center: NOAA Next Generation Radar (NEXRAD) Level 3 Products Hail Signatures, NOAA National Centers for Environmental Information, https://doi.org/10.7289/V5W9574V, accessed: 29 July 2019, 2019.

https://doi.org/10.5194/nhess-2019-342
Preprint. Discussion started: 27 November 2019

Oakley, N. S. and Redmond, K. T.: A climatology of 500-hPa closed lows in the northeastern Pacific Ocean, 1948–2011, Journal of Applied Meteorology and Climatology, 53, 1578–1592, https://doi.org/10.1175/JAMC-D-13-0223.1, 2014.

Oakley, N. S., Cannon, F., Munroe, R., Lancaster, J. T., Gomberg, D., and Ralph, F. M.: Brief communication: Meteorological and climatological conditions associated with the 9 January 2018 post-fire debris flows in Montecito and Carpinteria, California, USA, Natural Hazards and Earth System Sciences, 18, 3037–3043, https://doi.org/10.5194/nhess-18-3037-2018, 2018.

Price, C. and Rind, D.: What determines the cloud-to-ground lightning fraction in thunderstorms?, Geophysical Research Letters, 20, 463–466, https://doi.org/10.1029/93GL00226, 1993.

Price, C. G.: Lightning applications in weather and climate research, Surveys in Geophysics, 34, 755–767, https://doi.org/10.1007/s10712-012-9218-7, 2013.

Pruppacher, H. and Klett, J.: Microphysics of clouds and precipitation, Kluwer Acad, Morwell Mass, 1997.

Ralph, F. M., Rutz, J. J., Cordeira, J. M., Dettinger, M., Anderson, M., Reynolds, D., Schick, L. J., and Smallcomb, C.: A scale to characterize the strength and impacts of atmospheric rivers, Bulletin of the American Meteorological Society, https://doi.org/10.1175/BAMS-D-18-0023.1, 2019.

Saha, S., Moorthi, S., Wu, X., Wang, J., Nadiga, S., Tripp, P., Behringer, D., Hou, Y.-T., Chuang, H.-y., Iredell, M., et al.: The NCEP climate forecast system version 2, Journal of Climate, 27, 2185–2208, https://doi.org/10.1175/JCLI-D-12-00823.1, 2014.

USGS: Post-Fire Debris-Flow Hazards: Thomas Fire, https://landslides.usgs.gov/hazards/postfire_debrisflow/detail.php?objectid=178, accessed: 3 September 2019, 2019.

Wallace, J. M. and Hobbs, P. V.: Atmospheric science: an introductory survey, vol. 92, Elsevier, 2006.